Kinetics of O_2 Reduction at Illuminated TiO_2 Films

Samina Ahmed, Sofia M. Fonseca, Terence J. Kemp, and Patrick R. Unwin*

Department of Chemistry, University of Warwick, Coventry, CV4 7AL, U.K.

Received: March 7, 2003

The channel flow method with electrochemical detection (CFMED) has been used to investigate the photoelectrochemical reduction of O_2 at UV-illuminated TiO_2 surfaces in both aerated and oxygenated solutions. This approach detects O_2 amperometrically at a working detector electrode strategically positioned downstream of a TiO_2 surface, comprising a thin film of particulate material (Degussa P-25). By monitoring the transport-limited current as a function of flow rate with and without illumination, it has been possible to analyze the reaction kinetics in terms of various models proposed in the literature. The kinetics of the reduction process are reported, and the implications for semiconductor photocatalysis are discussed.

Introduction

TiO_2 particles, either in suspension[1] or deposited as thin films,[2] have been used widely to promote the photocatalytic degradation of various organic compounds in aqueous solution when irradiated with light of energy greater than the band gap of the semiconductor ($h\upsilon \geq E_{bg}$). For halogenated organics, partly of interest in this paper, the overall process can be written simply as[3]

$$\text{organic pollutant} + O_2 \xrightarrow[h\upsilon \geq E_{bg}]{\text{semiconductor}} CO_2 + H_2O + \text{mineral acids} \quad (1)$$

Despite countless studies of reaction 1, there is still no clear consensus on the complete mechanism or, indeed, the rate-limiting step. Many previous studies of reaction 1 have been analyzed in terms of a Langmuir−Hinshelwood (L−H) scheme,[3−5] but the adsorption constants for both O_2 and organic substrates on the semiconductor surface, derived from this model, have been found to be quite different from those measured independently.[3,6,7] Moreover, several investigations[8−10] have shown that a number of alternative mechanisms for the photomineralization process can lead to a rate law which is formally similar to that derived from the Langmuir−Hinshelwood model.

A key point in mechanistic studies of photomineralization processes concerns the role of oxygen. For photomineralization to proceed, the photogenerated electron must be scavenged by an electron acceptor, while the hole produced is involved in the oxidation of organic substrate, either directly or via $OH^{\bullet}$ formed by reaction with water. In the majority of cases, oxygen is employed as the electron scavenger. Since the quantum yields for photomineralization are low under conditions where the concentration of organic is small or the organic is not strongly adsorbed, an important question is the following: what factors limit the efficiency of the process? In particular, the role of electron transfer (ET) to oxygen has been the focus of attention in theoretical[11] and experimental[12] studies under steady-state conditions. The effect of oxygen for periodically illuminated systems[6] and electrochemically assisted photocatalysis[13] has also received attention. Theoretical models by Gerischer and Heller[11] led to the proposition that, in particulate systems, heterogeneous ET to oxygen would be slow, which has been confirmed in some experimental studies.[12] However, other investigations suggest that ET to oxygen may not be rate limiting.[14,15]

An interesting alternative approach to interpreting the kinetics of ET to O_2 was the application of a flux-matching condition by Lewis and co-workers[16] to describe the TiO_2-catalyzed photomineralization of organic substrates. The overall rate of the interfacial process was considered to be predetermined by the fact that, at steady state, the flux of holes across the solid/liquid interface must be balanced by an equivalent flux of electrons. Using single-crystal TiO_2 photoelectrodes, Lewis and co-workers determined the kinetics of O_2 reduction as a function of applied potential in the dark and compared the cathodic rates of reaction to the photoanodic current characteristics in the absence of oxygen. The approach provided an explanation as to why recombination in TiO_2-catalyzed photomineralization is significant.

The aim of this paper is to investigate the kinetics of O_2 reduction in a supported particulate TiO_2 system. As discussed above, much of the prior work on O_2 photoreduction at TiO_2 has been on particulate systems and there is little quantitative information on the factors controlling O_2 reduction at immobilized films. Our approach utilizes the channel flow method with electrochemical detection (CFMED), which has proven powerful for investigating kinetics at a variety of solid/liquid interfaces in the dark[17,18] and at illuminated electrode/solution interfaces.[19,20] We have recently demonstrated the utility of CFMED for monitoring product (Cl^-) formation and the effect of mass transport in the photomineralization of 4-chlorophenol.[21] The CFMED allows the investigation of reaction kinetics at solid/liquid interfaces by detecting products, intermediates, and reactants in solution at an electrode located downstream of a substrate of interest. The solid substrate and electrodes are located in one wall of a channel through which solution flows under well-defined (laminar), variable and calculable mass transport conditions. This approach permits the ready resolution of mass transport effects and interfacial kinetics. In this paper, we extend the method and demonstrate how the kinetics and mechanism of the photoelectrochemical reduction of oxygen at illuminated TiO_2 surfaces can be investigated. The approach described complements recent rotating disk studies of semiconductor photocatalysis at immobilized films of TiO_2,[22] which has explored oxygen diffusion limitations in controlling the kinetics of the reaction.

* To whom correspondence should be addressed. E-mail: p.r.unwin@warwick.ac.uk.

10.1021/jp030312z CCC: $25.00
Published on Web 05/23/2003

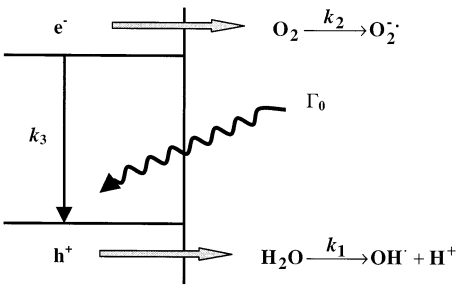

Figure 1. Schematic representation of surface electron and hole processes in the reduction of O_2 at illuminated TiO_2.

Theory

Mechanistic Model for the Photoreduction of O_2. We follow closely the basic idea in the earlier work of Lewis et al.[16] and consider the surface electron and hole processes in terms of the simplified schematic shown in Figure 1.

Under steady-state conditions, the balances for the photogenerated holes, h^+ and electrons, e^- are given by

$$\frac{d(h^+)}{dt} = 0 = \Gamma_0 - k_1(h^+) - k_3(e^-)(h^+) \tag{2}$$

$$\frac{d(e^-)}{dt} = 0 = \Gamma_0 - k_2(e^-)[O_2]_i - k_3(e^-)(h^+) \tag{3}$$

where $[O_2]_i$ refers to the oxygen concentration at the TiO_2/ water interface. In these equations, (h^+) and (e^-) denote the hole and electron concentrations, respectively. Γ_0 is the light intensity absorbed by TiO_2, which creates a flux of electrons and holes, and k_1 and k_2 are the rate constants for the transfer of holes and electrons, respectively, across the TiO_2/water interface. The rate constant for the recombination of electrons and holes is denoted by k_3.

Equation 2 is identical in form to eq 10 in ref 16 and assumes that water is exclusively involved as the hole acceptor. This is appropriate for the studies in this paper, which mainly consider systems comprising aerated or oxygenated aqueous solutions. Equation 3 is similar to eq 9 in ref 16, except that the second term on the right-hand side recognizes that the concentration of molecular oxygen close to the TiO_2/water interface, $[O_2]_i$, may differ from that in bulk solution. This is not an issue for the suspended particulate systems considered previously[16] but is important in supported catalyst systems where mass transport effects may be significant.

Additionally, we have to give some consideration as to whether the intermediates and products of the electron and hole transfer processes with O_2 and H_2O, respectively, will be involved in further surface electrochemical processes. Given the relatively low mass transport rates in immobilized film systems, compared to suspensions, it is reasonable to assume that the initial superoxide intermediate, $O_2^{\bullet -}$ may be readily reduced further to peroxide or even to hydroxide.[10]

$$O_2^{\bullet -} + 2H_2O + 3e^- \rightarrow 4OH^-$$

In the absence of any oxidizable species, hydroxyl radicals produced in the hole reaction are expected to dimerize readily to yield H_2O_2, which may undergo reduction with conduction band electrons[23,24] or oxidation (via h^+ or $^\bullet OH$) to water and O_2.[24] It is considered most likely that H_2O_2 is reduced at TiO_2.[25,26] The reactivity of H_2O_2 is certainly extensive since it has proved to be difficult to detect, except at small traces.[22,24,27,28] Indeed, in the experiments reported herein (see later), we were unable to detect H_2O_2 at any of the mass transport rates encountered. Moreover, we have carried out scanning electrochemical microscopy studies of O_2 reduction at illuminated TiO_2 surfaces (at open-circuit) and not detected H_2O_2 as an intermediate,[29] in agreement with similar work recently reported.[28]

Since these follow-up electron-transfer processes result from initial ET to O_2 (and the corresponding balancing anodic (h^+) process), and since these reactions appear to be relatively rapid on the channel flow time scale, eqs 2 and 3 provide an adequate description of the mass balance problem. The rate constant, k_2 then describes the net ET rate rather than the initial one-electron process.

As discussed below, we consider several cases to describe ET to O_2. Equation 3 represents the case where ET occurs to O_2 in solution. Equations 2 and 3 yield expressions for (h^+) and (e^-):

$$(h^+) = \frac{\Gamma_0}{k_1 + k_3(e^-)} \tag{4}$$

$$(e^-) = \frac{\Gamma_0}{k_2[O_2]_i + k_3(h^+)} \tag{5}$$

The flux of holes and electrons across the TiO_2/water interface balance, so the rate of oxygen reduction (or water oxidation), j is given by

$$j = \frac{k_1 k_2 [O_2]_i}{2k_3}\left[\left(1 + \frac{4\,\Gamma_0 k_3}{k_1 k_2 [O_2]_i}\right)^{1/2} - 1\right] \tag{6}$$

If

$$\frac{4\,\Gamma_0 k_3}{k_1 k_2 [O_2]_i} \gg 1$$

Equation 6 simplifies to

$$j = \left[\frac{k_1 k_2 \Gamma_0 [O_2]_i}{k_3}\right]^{1/2} \tag{7}$$

Equation 7 predicts that the rate of oxygen reduction should be half-order in the interfacial concentration of O_2 and the flux of electrons and holes in the bulk TiO_2, which are produced as a consequence of the light absorption process (directly related to the light flux intensity).

We also need to recognize that O_2 may adsorb at the TiO_2 surface prior to electron transfer. If adsorption is rapid, the concentration of surface bound oxygen will depend on the isotherm which describes the adsorption process, since the rate law for the reduction of oxygen becomes

$$j = \left(\frac{k_1 k_2' \Gamma_0 \Omega}{k_3}\right)^{1/2} \tag{8}$$

where Ω denotes the surface density of adsorbed O_2. The rate constant for the ET process is now denoted by k_2' to indicate a change in the nature of the reaction (and a corresponding change in the units for the rate constant).

The Langmuir isotherm is usually assumed for the adsorption of O_2 in photomineralization studies. Using this isotherm, eq 8 becomes

$$j = \left(\frac{k_1 k_2' \Gamma_0 \Omega_{max}}{k_3}\right)^{1/2} \left(\frac{K[O_2]_i}{1 + K[O_2]_i}\right)^{1/2} \quad (9)$$

where Ω_{max} denotes the maximum surface density of adsorbed O_2 and K is the equilibrium adsorption constant. It should be noted that the adsorption process is written in terms of the concentration of O_2 at the TiO_2/water interface. The demonstration that the interfacial concentration of O_2 may deviate significantly from the bulk value during the photoreduction process at immobilized TiO_2 is an outcome of the studies reported in this paper.

The limits to eq 9, $K[O_2]_i \ll 1$ and $K[O_2]_i \gg 1$, result in eqs 10 and 11, respectively,

$$j = \left(\frac{k_1 k_2' \Gamma_0 \Omega_{max} K[O_2]_i}{k_3}\right)^{1/2} \quad (10)$$

$$j = \left(\frac{k_1 k_2' \Gamma_0 \Omega_{max}}{k_3}\right)^{1/2} \quad (11)$$

Equation 10 has the same form as that of eq 7, while eq 11 suggests a zeroth-order dependence on $[O_2]_i$.

As an alternative to the approach of Lewis et al.,[16] it is also worth assessing whether a simple Langmuir model describes the process, as adopted for the treatment of photomineralization kinetics.[3] In this case, the rate law has the form

$$j = \frac{k' K[O_2]_i}{1 + K[O_2]_i} \quad (12)$$

where k' is a rate constant for the heterogeneous ET process.

The limits in eq 12 result in first- and zeroth-order dependences on the interfacial O_2 concentration for $K[O_2]_i \ll 1$ and $K[O_2]_i \gg 1$, respectively,

$$j = k' K[O_2]_i \quad (13)$$

$$j = k' \quad (14)$$

If the adsorption step were rate-limiting, a rate law with a first-order dependence on $[O_2]_i$ might be expected and would be of the form

$$j = k''[O_2]_i(1 - \theta) \quad (15)$$

where k'' is a heterogeneous rate constant for adsorption and θ is the fraction of filled surface sites. Since the assumption of adsorption as the rate-limiting step implies that the follow-up steps are rapid, and since the products are soluble, $\theta \rightarrow 0$ and

$$j = k''[O_2]_i \quad (16)$$

Mass Transport Model for CFMED. A cross section of the setup used for the oxygen photoreduction studies is shown schematically in Figure 2. Practical cells for channel flow studies are designed so that the height, $2h$ is much less than the width, d. Moreover, the width w of the reacting interface is related to d as $w < d$, so that the two-dimensional flow over the interface(s) of interest can be considered. Under fully developed laminar (Poiseuille) flow conditions, in the steady-state limit, the transport of dissolved oxygen in the aqueous phase is governed by[18]

$$D\frac{\partial^2[O_2]}{\partial y^2} = v_0\left[1 - \frac{(y-h)^2}{h^2}\right]\frac{\partial[O_2]}{\partial x} \quad (17)$$

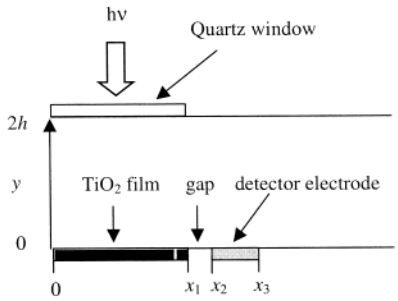

Figure 2. Setup and coordinate system used to model mass transport in CFMED.

TABLE 1: Boundary Conditions at the TiO_2/Aqueous Interface for the Five Kinetic Cases of Interest

case	boundary condition at the TiO_2/aqueous interface ($y = 0$, $0 \le x < x_1$)
1	$D\frac{\partial[O_2]}{\partial y} = k_{case1}[O_2]^{1/2}$
2	$D\frac{\partial[O_2]}{\partial y} = k_{case2}$
3	$D\frac{\partial[O_2]}{\partial y} = k_{case3}\left(\frac{[O_2]}{1 + K[O_2]}\right)^{1/2}$
4	$D\frac{\partial[O_2]}{\partial y} = k_{case4}\left(\frac{[O_2]}{1 + K[O_2]}\right)$
5	$D\frac{\partial[O_2]}{\partial y} = k_{case5}[O_2]$

The x and y coordinates are defined in Figure 2. D is the diffusion coefficient of O_2, and v_0 is the fluid velocity in the center of the channel. This latter variable is related to the experimental volume flow rate, V_f by

$$v_0 = \frac{3V_f}{4\,hd} \quad (18)$$

The various rate laws described in the previous section constitute the boundary conditions at the TiO_2 surface ($y = 0$, $0 \le x < x_1$). In total, five cases arise, which are summarized in Table 1. Case 1 is the limiting rate law derived from eqs 7 and 10, and the simplified rate constant k_{case1} can be related to various parameters by comparing this boundary condition directly with eqs 7 and 10. The zeroth-order dependence of the oxygen flux at the TiO_2/water interface, case 2, derives from eqs 11 and 14. Case 3 relates to eq 9, while case 4 is the boundary condition corresponding to eq 12. Finally, case 5 can be derived from either eq 13 or eq 16.

The other boundary conditions that need specifying are

$$y = 0, \quad x_1 < x \le x_2: \quad D\frac{\partial[O_2]}{\partial y} = 0 \quad (19)$$

$$y = 0, \quad x_2 < x \le x_3: \quad [O_2] = 0 \quad (20)$$

$$y = 2h, \quad 0 < x: \quad D\frac{\partial[O_2]}{\partial y} = 0 \quad (21)$$

$$x < 0, \quad \text{all } y: \quad [O_2] = [O_2]^* \quad (22)$$

where the superscripted asterisk signifies the bulk concentration.

Equation 20 relates to the detector electrode and corresponds to diffusion-limited amperometric detection of O_2. The current

is calculated from

$$I_{lim} = nFDw\int_{x_2}^{x_3} \frac{\partial[O_2]}{\partial y}\,dx \qquad (23)$$

where I_{lim} is transport-limited current at the detector electrode, n is the number of electrons transferred in the electrode process, F is Faraday's constant, and w denotes the width of the detector electrode. It is convenient to define the shielding factor S_f, which is the ratio of currents at the detector electrode when there is a reaction (light on) and no reaction (light off):

$$S_f = \frac{I_{lim}(\text{light on})}{I_{lim}(\text{light off})} \qquad (24)$$

For the band detector electrodes, used in the studies herein, the denominator is given by the Levich equation:

$$I_{lim} = 0.925nFw\left(\frac{D^2l^2V_f}{h^2d}\right)^{1/3}[O_2]^* \qquad (25)$$

where l is the length of the detector electrode ($x_3 - x_2$).

The problems outlined above were solved using the backward implicit finite difference method, which has been applied extensively to various steady-state CFMED problems.[17] The present problem presents no additional conceptual or computational complexities.

Experimental Section

Chemicals. $NaC1O_4 \cdot H_2O$ (A.R., BDH), 4-chlorophenol (4-CP, Aldrich, 99%), and TiO_2 (Degussa P25) were used as received. Aqueous solutions were prepared from Milli-Q (Millipore Corp.) reagent grade water (resistivity 18 MΩ cm), and experiments were carried out using either aqueous aerated or oxygenated solutions of 0.1 M $NaC1O_4$.

Preparation and Characterization of TiO_2 Films. TiO_2 films were prepared and characterized as described recently.[21] In brief, 5 g of TiO_2 was mixed with 100 mL of Milli-Q water, sonicated for 1 h, and stirred for 5 h with a magnetic stirrer. The suspension was dropped onto the glass surface of a cell coverplate (described below) and then dried with a stream of Ar gas. This process was typically repeated five times to achieve an even, complete coating. The coverplate was dried in an oven at 373 K for 12 h, resulting in a mechanically stable, optically opaque film, with a thickness of ca. 10 μm.

Assembly of the Channel Flow Cell and Procedure. The basic assembly of the flow cell for interfacial photochemical experiments has been described in detail previously.[21] The same type of cell was used for the present studies, except that an Ag or Pt band electrode, described below, operated as an amperometric detector. The cell, pictured in Figure 3, comprised three parts: (i) a channel inlet−outlet unit fabricated from PVC, with a quartz window to permit illumination; (ii) a coverplate containing electrodes and a glass plate onto which a thin TiO_2 film could be deposited; and (iii) a 0.50 mm thick Teflon spacer producing a channel 12 mm wide and 45 mm long.

For the majority of experiments, amperometric detection of O_2 was accomplished using an Ag band electrode (2.90 mm wide and 0.25 mm long) positioned downstream of the glass plate. For a few experiments where the anodic, as well as cathodic, potential windows were of interest, this was replaced by a Pt electrode of similar dimensions. The width of the detector electrode was much less than the channel width to allow the

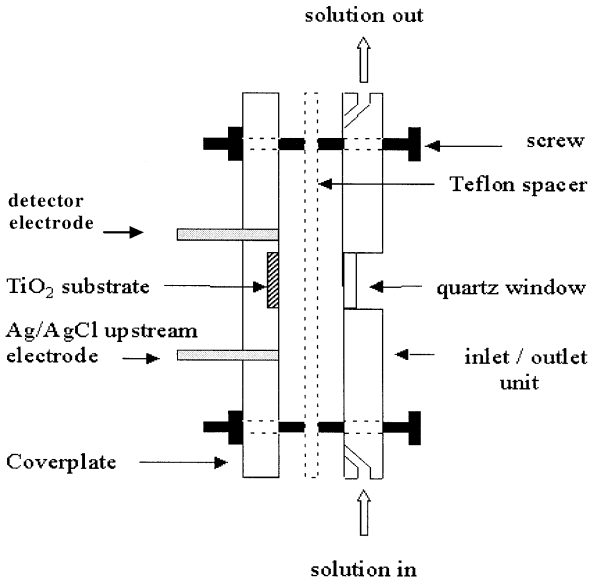

Figure 3. Cross section of the channel flow cell used to investigate the photoreduction of O_2 at TiO_2. The auxiliary electrode is not shown.

modeling of mass transport in terms of two-dimensional convective diffusion,[17,21] consistent with the model presented earlier. The downstream detector electrode was located ca. 2.00 mm away from the end of the TiO_2 interface region in a location where there was no direct illumination. A 1.00 mm diameter Ag wire was placed flush in the plate, 7.50 mm upstream of the glass plate as a reference electrode and all potentials are quoted with respect to this electrode. A piece of Pt foil (6.0 mm wide, 3.0 mm long, placed downstream of the microband detector electrode) functioned as a counter electrode in a conventional three-electrode arrangement. The precise height of the assembled cell was determined as outlined previously.[30]

Prior to each set of experiments, the coverplate was polished flat using a series of finer diamond lapping compounds (25−1 μm; Kemet International, UK) and 0.05 μm alumina (Buehler, Lake Bluff, IL). Flow through the cell was achieved using a dual drive syringe pump (model 200, CP Instruments, Bishops Stortford, Hertfordshire, UK), and the flow cell was shielded from any electrical noise using a Faraday cage. For experiments under 1 atm O_2, solutions were purged with O_2 (99.5%, BOC) and the pump was placed inside an "atmos bag" (Aldrich, Milwaukee, WI) into which O_2 was passed. The flow tubing (1.5 mm id, Omnifit) was jacketed with PVC tubing (12 mm id) through which a continuous flow of O_2 was maintained.

Illumination was achieved with a high power xenon lamp (Illuminator 6000, Eurosep Instruments, Cergy-Pontoise, France). An infrared quartz filter filled with $CuSO_4$ solution was employed to prevent heating of the cell during irradiation. The intensity of the lamp was controlled via different output settings available and also by the use of neutral density filters (New Focus, San Jose, CA). A modification of the method developed by Hatchard and Parker[31] was followed to determine the light flux intensity, while a full emittance profile of the lamp was determined by Vincze et al.[31b] The apparent light flux density of ultraband gap photons Γ_o for the TiO_2 photosensitized process of interest herein was in a typical range of $(0.74-3.9) \times 10^{17}$ q cm^{-2} s^{-1}.

Amperometric detection of O_2 was accomplished with a potentiostat and triangular wave generator (Oxford Electrodes, UK). Steady-state voltammograms and transport-limited current−time data were acquired, as a function of flow rate, using

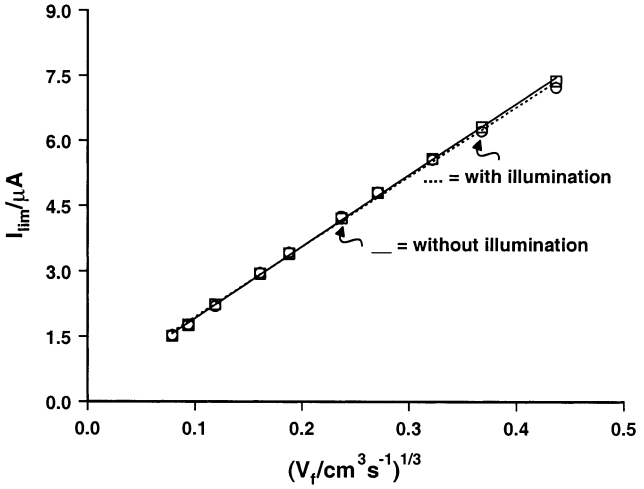

Figure 4. Levich plot for the reduction of O_2 at a channel Ag band electrode in the dark (□) and with UV-illumination of the zone upstream of the electrode (○). The best fits of the data to the Levich equation are shown as dotted (with illumination) and solid (without illumination) lines.

a PC-Lab data acquisition board (National Instruments, Austin, TX) in a personal computer, using software written in-house by Dr. N. J. Evans.

Results and Discussion

Effect of Illumination on [O_2] Downstream of a TiO_2 Surface. Preliminary amperometric measurements were made at an Ag microband channel electrode, while flowing aerated 0.1 M $NaClO_4$ aqueous solution at flow rates in the range $5.0 \times 10^{-4}-1.0 \times 10^{-1}$ cm^3 s^{-1}. Voltammograms for the reduction of O_2 were recorded both in the dark and with UV-illumination at a light flux intensity of 3.9×10^{17} q cm^{-2} s^{-1}, initially without any TiO_2 film present. The detector electrode potential E was scanned at a rate of 10−20 mV s^{-1} from −0.1 V, where no Faradaic electrode reaction occurred, to −0.8 V, well beyond the potential where the current reached a limiting steady state. Steady-state transport-limited currents, obtained at a range of flow rates, were analyzed in terms of the Levich equation (eq 25).

Typical results are shown in Figure 4, which demonstrate the required cube-root dependence of the limiting currents on volume flow rate with both illumination of the cell and in the dark. Analysis of the slopes of the plots suggests a four-electron process, as found at Ag disk microelectrodes.[32] The similarity of the behavior observed in the dark and light indicates that UV-illumination of the solution in the absence of TiO_2 has little effect on the concentration of [O_2]. Moreover, the coincidence of the data at low flow rates, in particular, confirms that convective flow of the solution minimizes possible complications from heating effects due to irradiation, which is a recognized benefit of channel electrode methodology.[19]

Further assessment of the CFMED approach was carried out in the presence of a TiO_2 film via the front-illumination of the reagent solution with a similar range of flow rates. Typical voltammetric curves are shown in Figure 5. The voltammograms in Figure 5a, recorded with a flow rate of 8.33×10^{-4} cm^3 s^{-1}, show a significant diminution of the limiting current signal for O_2 reduction at the detector electrode when the TiO_2 film is irradiated. The voltammogram with illumination can be confidently assigned to O_2 reduction alone without any detectable contribution from H_2O_2 produced at the TiO_2 surface. This was confirmed with experiments using a Pt detector electrode, which yielded similar cathodic effects to those described, but no anodic

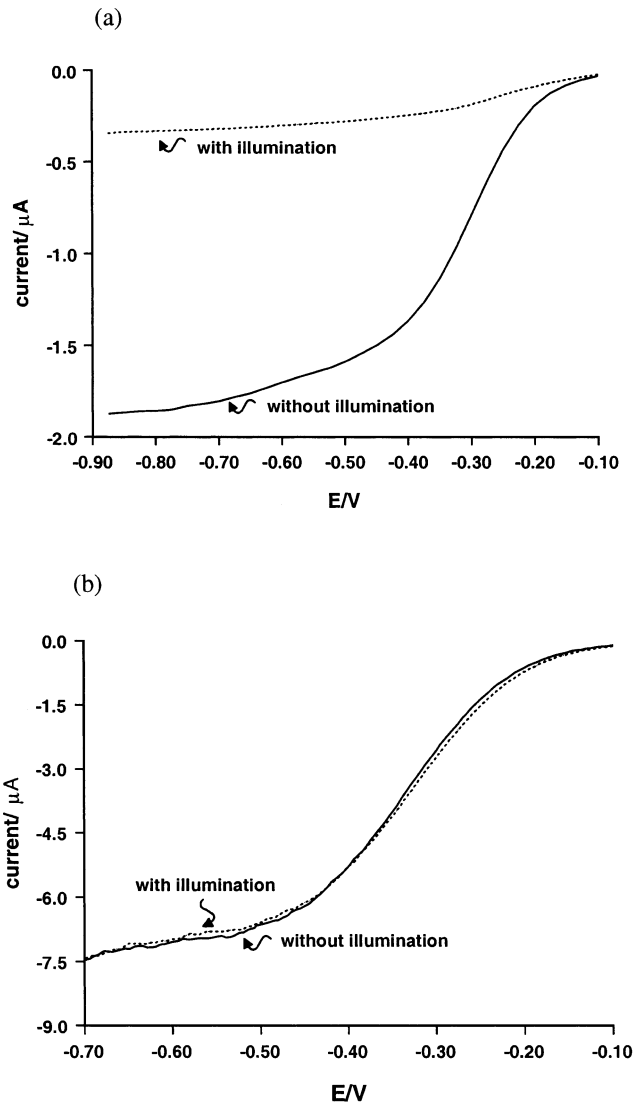

Figure 5. Voltammograms for the reduction of O_2 at an Ag electrode, downstream of a TiO_2 surface with (···) and without (—) illumination. The solution contained 0.1M $NaClO_4$ and atmospheric O_2, while the data are for flow rates of (a) 8.33×10^{-4} cm^3 s^{-1} and (b) 0.133 cm^3 s^{-1}. $\Gamma_o = 3.9 \times 10^{17}$ q cm^{-2} s^{-1}.

signal was detectable that would be expected should H_2O_2 reach the detector electrode.

Figure 5b indicates that O_2 depletion at the illuminated TiO_2 surface is strongly flow-rate dependent, since at very high flow rate ($V_f = 0.133$ cm^3 s^{-1}) there is little change in limiting current at the detector electrode when the TiO_2 surface is illuminated. It may be deduced that the effects are kinetic; at very slow flow rate the transit time over the illuminated zone is longest, resulting in significant reaction of oxygen at the TiO_2 surface and consequently a lower fraction reaching the detector electrode.

Reduction of O_2 at TiO_2 Films: Kinetics under Aerated (0.2 atm O_2) Conditions. A number of experiments were carried out with the light flux intensity range defined. An aerated aqueous solution of 0.1M $NaClO_4$ was flowed through the cell, with flow rates in the range $5.0 \times 10^{-4}-1.0 \times 10^{-1}$ cm^3 s^{-1}, and shielding factors (eq 24), obtained from the data, were analyzed using the theoretical models described earlier. As an example case, data obtained at an intensity $\Gamma_o = 0.95 \times 10^{17}$ q cm^{-2} s^{-1} are analyzed in terms of all the models in Figure 6. Figure 6a shows the best simulated fits to the simple first-order

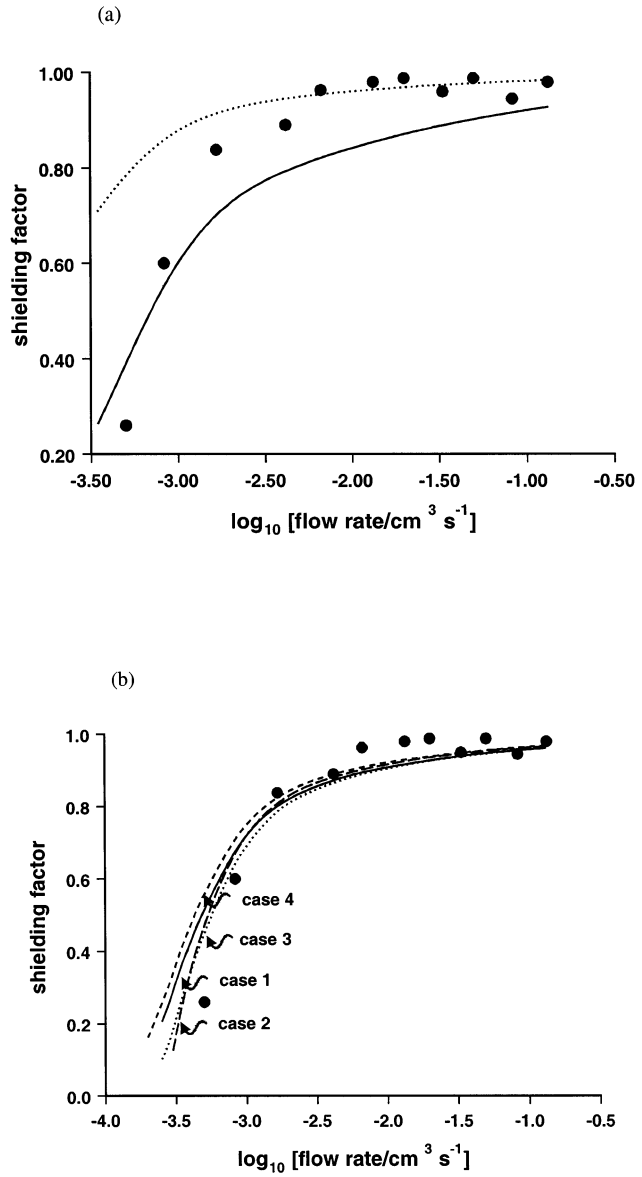

Figure 6. Detection of O_2 (●) downstream of an illuminated TiO_2 surface as a function of log (flow rate/cm^3 s^{-1}). The best fits are shown for: (a) case 5 (solid line with $k_{case5} = 5.0 \times 10^{-4}$ cm s^{-1} and dotted line with $k_{case5} = 1.0 \times 10^{-4}$ cm s^{-1}); (b) the remaining cases with corresponding rate constants $k_{case1} = 1.2 \times 10^{-7}$ mol$^{1/2}$ cm$^{-1/2}$ s^{-1}, $k_{case2} = 0.50 \times 10^{-10}$ mol cm^{-2} s^{-1}, $k_{case3} = 0.63 \times 10^{-10}$ mol cm^{-2} s^{-1}, and $k_{case4} = 0.79 \times 10^{-10}$ mol cm^{-2} s^{-1}. $\Gamma_o = 0.95 \times 10^{17}$q cm^{-2} s^{-1}.

model (case 5). This is seen to provide a poor description of the shielding factor−flow rate characteristics. With a rate constant of 1.0×10^{-4} cm s^{-1}, the theory matches the experimental data in the high flow rate region but deviates significantly from the data obtained at low flow rates. A rate constant of 5.0×10^{-4} cm s^{-1} is needed to approach the low flow rate data, but this produces a poor fit for all other flow rates considered. The fits to case 5 for all of the other experiments undertaken were also unsatisfactory, so this case was not considered further.

Figure 6b shows that the remaining cases ($k_{case1} = 1.2 \times 10^{-7}$ mol$^{1/2}$ cm$^{-1/2}$ s^{-1}, $k_{case2} = 0.50 \times 10^{-10}$ mol cm^{-2} s^{-1}, $k_{case3} = 0.63 \times 10^{-10}$ mol cm^{-2} s^{-1}, and $k_{case4} = 0.72 \times 10^{-7}$ mol cm^{-2} s^{-1}) produce reasonably good agreement with the experimental data over the entire range of flow rates studied. However, to simulate the shielding factors numerically, cases 3 and 4 require an equilibrium adsorption constant for O_2. A

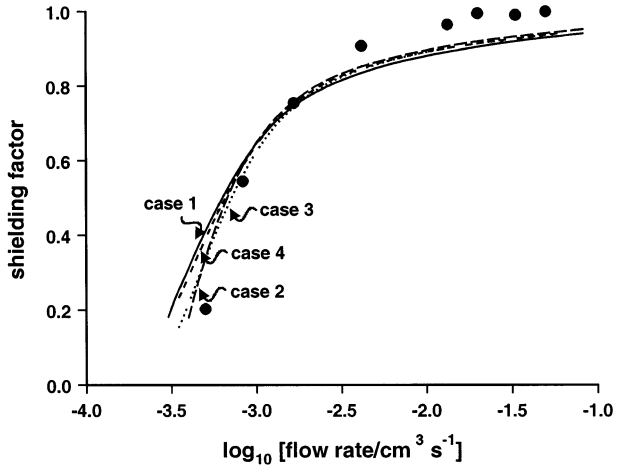

Figure 7. Detection of O_2 (●) downstream of an illuminated TiO_2 surface as a function of log (flow rate/cm^3 s^{-1}). The best fits are shown for $k_{case1} = 1.6 \times 10^{-7}$ mol$^{1/2}$ cm$^{-1/2}$ s^{-1} $k_{case2} = 0.63 \times 10^{-10}$ mol cm^{-2} s^{-1}, $k_{case3} = 0.81 \times 10^{-10}$ mol cm^{-2} s^{-1}, and $k_{case4} = 0.99 \times 10^{-10}$ mol cm^{-2} s^{-1}. $\Gamma_o = 1.50 \times 10^{17}$ q cm^{-2} s^{-1}.

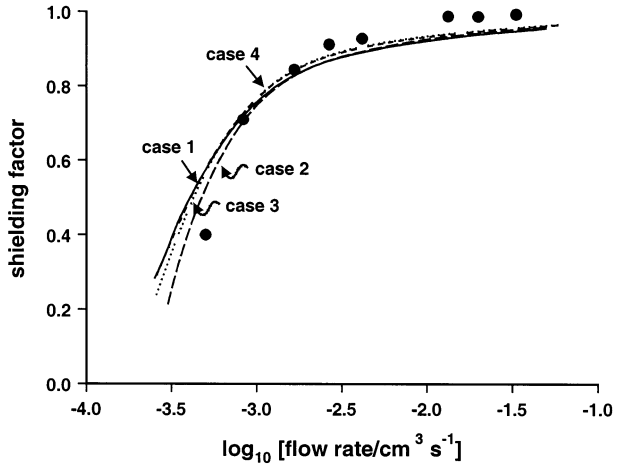

Figure 8. Detection of O_2 (●) downstream of an illuminated TiO_2 surface as a function of log (flow rate/cm^3 s^{-1}). The best fits are shown for $k_{case1} = 1.0 \times 10^{-7}$ mol$^{1/2}$ cm$^{-1/2}$ s^{-1}, $k_{case2} = 0.45 \times 10^{-10}$ mol cm^{-2} s^{-1}, $k_{case3} = 0.48 \times 10^{-10}$ mol cm^{-2} s^{-1}, and $k_{case4} = 0.60 \times 10^{-10}$ mol cm^{-2} s^{-1}. $\Gamma_o = 0.74 \times 10^{17}$ q cm^{-2} s^{-1}.

literature value[33] of $K = 9.63 \times 10^6$ cm^3 mol^{-1} was used for the present numerical simulations, which appears to be most appropriate.[29] In contrast, the zeroth-order and half-order simulations (cases 1 and 2) require only one parameter to fit the data.

Experimental shielding factors obtained over the range of light flux intensities of interest were compared alongside the best fit theoretical simulations for cases 1−4. Typical fits are shown in Figures 7 and 8 for light fluxes of 1.50×10^{17} and 0.74×10^{17} q cm^{-2} s^{-1}, respectively. The resulting rate constants are summarized in Table 2. It can be seen that all models provide a reasonable description of the behavior observed, with the shielding factor tending to unity at high flow rate and decreasing as the flow rate decreases. When Γ_o increases (compare Figure 7 with Figure 8), the value of the shielding factor is lower for a given flow rate (particularly noticeable in the low flow rate region). This is reflected by the trend of increasing rate constant with increasing Γ_o (Table 2).

The half-order model (case 2) predicts that the observed rate constant should depend on the square root of the light flux intensity (eq 10). To determine whether this applied, a plot of log k_{case1} vs log Γ_o was constructed, shown in Figure 9. A linear

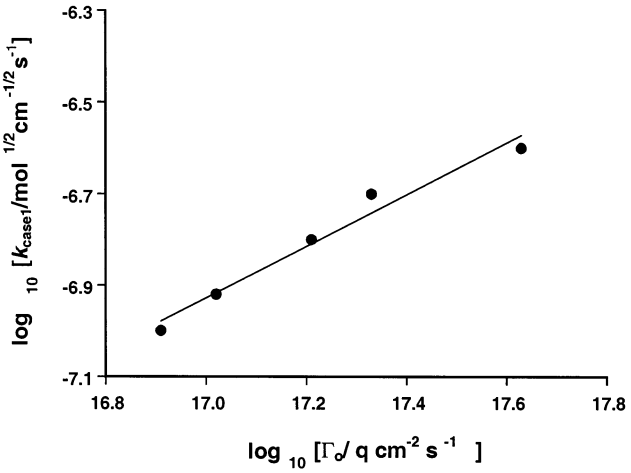

Figure 9. Plot of log k_{case1}vs log Γ_o.

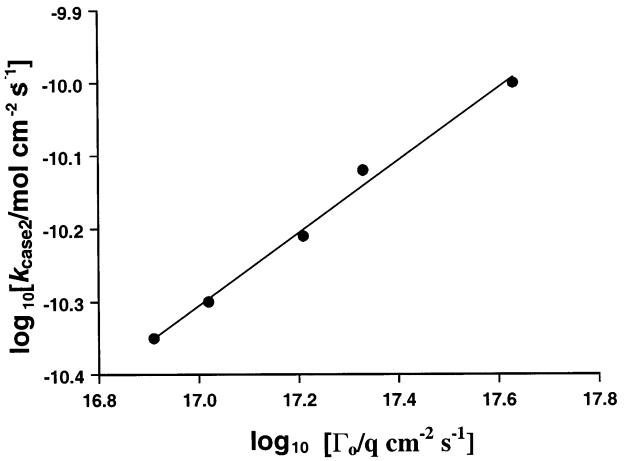

Figure 10. Plot of log k_{case2} vs log Γ_o.

TABLE 2: Values for the Rate Constants (Cases 1−4) Obtained from the Best-Fit Simulations for O_2 Photoreduction at TiO_2 in 0.1 M $NaClO_4$ under Aerated Conditions

Γ_o/q cm^{-2} s^{-1}	k_{case1}/mol$^{1/2}$ cm$^{-1/2}$ s^{-1}	k_{case2}/mol cm^{-2} s^{-1}	k_{case3}/mol cm^{-2} s^{-1}	k_{case4}/mol cm^{-2} s^{-1}
3.9×10^{17}	2.5×10^{-7}	1.0×10^{-10}	1.5×10^{-10}	1.9×10^{-10}
1.9×10^{17}	2.0×10^{-7}	0.75×10^{-10}	1.0×10^{-10}	1.3×10^{-10}
1.5×10^{17}	1.6×10^{-7}	0.63×10^{-10}	0.81×10^{-10}	0.99×10^{-11}
0.95×10^{17}	1.2×10^{-7}	0.50×10^{-10}	0.63×10^{-10}	0.79×10^{-11}
0.74×10^{17}	1.0×10^{-7}	0.45×10^{-10}	0.48×10^{-10}	0.60×10^{-11}

relationship is clearly evident, with a gradient of 0.56, which is close to the value predicted theoretically. The zeroth-order model (case 2) arises from the simple Langmuir model for $K[O_2] \gg 1$ (eq 14) and is a limit of the flux-matching model (eq 11). The latter predicts a half-order dependence of the rate constant on light intensity and the plot of log k_{case2} vs log Γ_o in Figure 10, giving a slope of 0.50. Likewise, the rate constants for cases 3 and 4 show a clear half-order dependence on intensity rate rather than first-order.

Effect of Organic Substrate. For comparative purposes it was considered interesting to investigate the photoelectrochemical reduction kinetics of O_2 in an aqueous solution of the organic substrate. The analysis of Lewis et al.[16] suggested that water would be the main reactant with photogenerated holes and that organic substrate would have little effect on enhancing the rate of hole capture and, consequently, the reduction of O_2 (within the flux matching model). Figure 11 represents the shielding factor−flow rate response for O_2 detection in an aerated aqueous

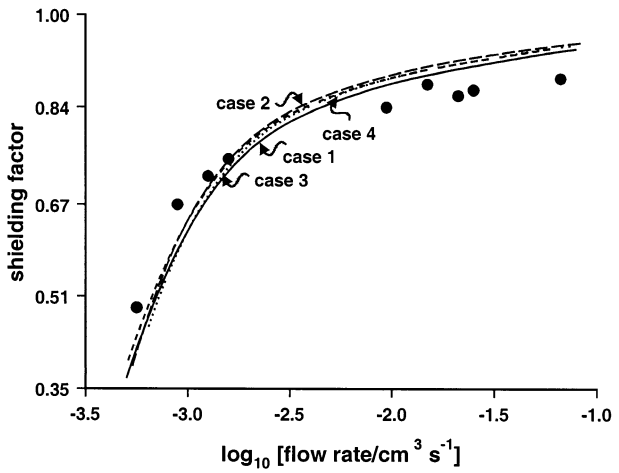

Figure 11. Detection of O_2 (●) downstream of an illuminated TiO_2 surface in 1.0 mM 4-CP with 0.1 M $NaClO_4$ as a function of log (flow rate /cm^3 s^{-1}). The best fits are shown for $k_{case1} = 1.5 \times 10^{-7}$ mol$^{1/2}$ cm$^{-1/2}$ s^{-1}, $k_{case2} = 0.60 \times 10^{-10}$ mol cm^{-2} s^{-1}, $k_{case3} = 0.80 \times 10^{-10}$ mol cm^{-2} s^{-1}, and $k_{case4} = 1.0 \times 10^{-10}$ mol cm^{-2} s^{-1}. $\Gamma_o = 0.97 \times 10^{17}$ q cm^{-2} s^{-1}.

solution of 4-CP (1 mM) containing 0.1 M $NaClO_4$ at $\Gamma_o = 0.97 \times 10^{17}$ q cm^{-2} s^{-1}. All models produce good fits to the experimental data and the simulated rate constants ($k_{case1} = 1.5 \times 10^{-7}$ mol$^{1/2}$ cm$^{-1/2}$ s^{-1}, $k_{case2} = 0.60 \times 10^{-10}$ mol cm^{-2} s^{-1}, $k_{case3} = 0.80 \times 10^{-10}$ mol cm^{-2} s^{-1}, and $k_{case4} = 1.0 \times 10^{-11}$ mol cm^{-2} s^{-1}) are in close agreement with those obtained for the reaction in 0.1 M $NaClO_4$ under a similar light flux density ($\Gamma_o = 0.95 \times 10^{17}$ q cm^{-2} s^{-1}, Table 1). Notice, however, that the slightly higher shielding factors at low flow rate suggest that 4-CP may have a slight inhibiting effect on the O_2 reduction kinetics. There is also a greater possibility that H_2O_2 may be produced at enhanced levels in the presence of organic substrate,[23−25] thereby contributing to the cathodic limiting current measurements.

It is also worth comparing the rate of O_2 consumption at the illuminated TiO_2 surface with the rate of Cl^- formation in the photomineralization process at a similar light intensity, since this comparison has rarely been made despite the possible link between the two processes. We have recently used the CFMED in potentiometric mode to probe Cl^- fluxes during the photomineralization of 4-CP under similar conditions to the O_2 reduction studies in this paper.[21,34] The zeroth-order rate constant $k_{case2} = 0.50 \times 10^{-10}$ mol cm^{-2} s^{-1} at $\Gamma_o = 0.95 \times 10^{17}$ q cm^{-2} s^{-1}, which describes the flux for O_2 loss, is similar to the zeroth-order rate constant (flux) of Cl^- formation in 1.0 mM 4-CP with 0.1 M $NaClO_4$, (0.40×10^{-10} mol cm^{-2} s^{-1}).[21,34] This close correlation provides evidence for the flux matching description of semiconductor-sensitized photomineralization processes.

Reduction of O_2 at TiO_2 Films: 1.0 atm O_2 Conditions. Examining the photoreduction at a different O_2 concentration is useful, since it may provide additional information on the rate law describing the process: case 1 predicts a half-order dependence of the flux on interfacial $[O_2]$, while case 2 predicts a flux that is independent of $[O_2]$. The rate constants for cases 3 and 4 should be independent of $[O_2]$. Several experiments were thus carried out in oxygenated $NaClO_4$ (0.1 M) solutions with Γ_o varied in the range $(1.5-3.9) \times 10^{17}$q cm^{-2} s^{-1}. Experimental results were analyzed in terms of cases 1−4, with typical data shown in Figure 12. The resulting rate constants, derived from best fit analyses, are summarized in Table 3. Comparison of these rate constants with the corresponding

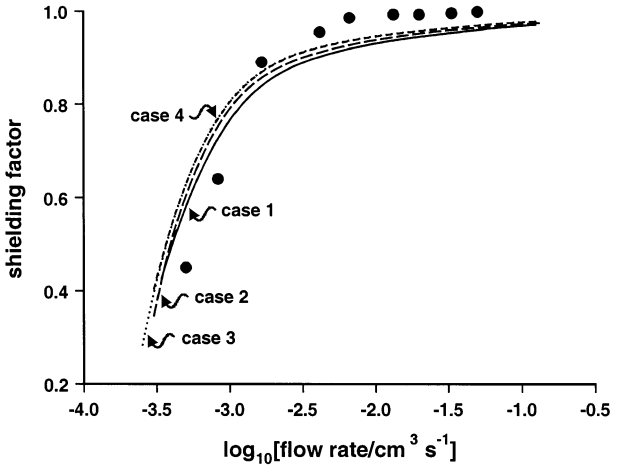

Figure 12. Detection of O_2 (●) downstream of an illuminated TiO_2 surface as a function of log (flow rate/cm^3 s^{-1}). The best fits are shown for $k_{case1} = 2.0 \times 10^{-7}$ mol$^{1/2}$ cm$^{-1/2}$ s^{-1}, $k_{case\ 2} = 1.9 \times 10^{-10}$ mol cm^{-2} s^{-1}, $k_{case3} = 1.7 \times 10^{-10}$ mol cm^{-2} s^{-1}, and $k_{case4} = 1.8 \times 10^{-10}$ mol cm^{-2} s^{-1}. $\Gamma_o = 1.9 \times 10^{17}$ q cm^{-2} s^{-1}.

TABLE 3: Values for the Rate Constants (Cases 1−4) Obtained from the Best-Fit Simulations for O_2 Photoreduction at TiO_2 in 0.1 M $NaClO_4$ under Oxygenated Conditions

Γ_o/q cm^{-2} s^{-1}	k_{case1}/mol $^{1/2}$ cm $^{-1/2}$ s^{-1}	k_{case2}/mol cm^{-2} s^{-1}	k_{case3}/mol cm^{-2} s^{-1}	k_{case4}/mol cm^{-2} s^{-1}
3.9×10^{17}	2.2×10^{-7}	2.3×10^{-10}	2.5×10^{-10}	2.6×10^{-10}
1.9×10^{17}	2.0×10^{-7}	1.9×10^{-10}	1.7×10^{-10}	1.8×10^{-10}
1.5×10^{17}	1.6×10^{-7}	1.6×10^{-10}	1.6×10^{-10}	1.7×10^{-10}

aerated rate constants (Table 1) clearly shows that the half-order model (case 1) provides a very consistent analysis. The significant increase in the value of k_{case2}, which occurs when the bulk oxygen concentration is increased, demonstrates that the order of the reaction with respect to O_2 is greater than zero. Consequently, cases 3 and 4, which are full Langmuir−Hinshelwood treatments, provide a better description, but there is still a notable increase in the rate constant for these cases when the oxygen concentration is increased. This suggests that, with the literature value of the oxygen adsorption constant, these models do not provide the optimal description of the oxygen reduction process. Although other adsorption constants have been suggested,[6a,35] these have been derived from kinetic analyses on the basis of assumed mechanisms and there is a need for more reliable independent data on oxygen adsorption at TiO_2. The results of this study suggest that case 1 provides the simplest description of the photoreduction process under the conditions of the experiments herein.

Quantum Efficiency of the Photoelectrochemical Reduction of O_2. It is apparent from the discussion above that case 1 provides the best description of the data, and it is worth estimating the maximum quantum efficiency Φ for the O_2 reduction process from the following expression related to this case.

$$\Phi = \frac{k_{case1}([O_2]^*)^{1/2}}{\Gamma_0} \qquad (26)$$

The results of this analysis are compiled in Table 4 for both aerated and oxygenated conditions. The overall quantum efficiencies are low because eq 26 does not account for scattering losses and the experiments reported have been carried out in the absence of any organic substrate. The maximum quantum efficiency (in the limit of fast flow rate) decreases as the light flux intensity increases due to the half-order dependence of the charge-transfer process on light flux (eq 7). This equation also explains the increase in quantum efficiency of the photoreduction process with an increase in O_2 concentration.

TABLE 4: Apparent Maximum Quantum Yields of O_2 Photoreduction at TiO_2 Films

(a) Aerated (0.2 atm O_2) Conditions

[substrate solution]	Γ_o/q cm^{-2} s^{-1}	Φ(%)
0.1 M $NaClO_4$	3.9×10^{17}	0.020
0.1 M $NaClO_4$	1.9×10^{17}	0.030
0.1 M $NaClO_4$	1.5×10^{17}	0.032
0.1 M $NaClO_4$	0.95×10^{17}	0.038
0.1 M $NaClO_4$	0.74×10^{17}	0.041
1 mM 4-CP in 0.1 M $NaClO_4$	0.97×10^{17}	0.037

(b) Oxygenated (1.0 atm O_2) Conditions

[substrate solution]	Γ_o/q cm^{-2} s^{-1}	Φ (%)
0.1 M $NaClO_4$	3.9×10^{17}	0.038
0.1 M $NaClO_4$	1.9×10^{17}	0.069
0.1 M $NaClO_4$	1.5×10^{17}	0.072

Conclusions

The amperometric detection mode of the CFMED has allowed the photoelectrochemical reduction kinetics of dissolved aqueous O_2 at a supported TiO_2 surface to be investigated. We have demonstrated that there is a flow-rate-dependent depletion of $[O_2]$ at illuminated TiO_2 surfaces, which is most significant at slow flow rates. This insight should provide a better understanding of the role of O_2 in photomineralization kinetics. Of the five models considered for the O_2 photoreduction kinetics, case 1 is able to explain all of the features observed experimentally with only one adjustable parameter. This model derives from the flux-matching approach,[16] outlined earlier in the paper.

The rate of O_2 consumption in 4-CP solutions has been found to be consistent with the rate of Cl^- formation under similar experimental conditions, supporting the idea that in the photomineralization process there is a balance in the rates of the anodic process (hole consumption generating hydroxyl radicals) and cathodic process (electron consumption by O_2).

Acknowledgment. We thank the Ministry of Science and Technology, Government of Bangladesh, for a scholarship for S.A. and the Portugeuese Foundation for Science and Technology for a scholarship for S.M.F. We are grateful to Dr. Claire Jones for preliminary experiments.

References and Notes

(1) (a) Cunningham, J.; Sedlak, P. *J. Photochem. Photobiol., A* **1994**, *77*, 255. (b) Serra, F.; Trillas, M.; Garcia, J.; Domènech, X. *J. Environ. Sci. Health* **1994**, *A29*, 1409. (c) D'Oliveira, J.-C.; Minero, C.; Pelizzetti, E.; Pichat, P. *J. Photochem. Photobiol., A* **1993**, *72*, 261. (d) Matthews, R. W. *Water Res.* **1990**, *24*, 653. (e) Rideh, L.; Wahrer, A.; Ronze, D.; Zoulalian, A. *Ind. Eng. Chem. Res.* **1997**, *36*, 4712. (f) Mills, A.; Morris, S.; Davies, R. *J. Photochem. Photobiol., A* **1993**, *70*, 183. (g) Mills, A.; Morris, S. *J. Photochem. Photobiol., A* **1993**, *71*, 75.

(2) (a) Bryne, J. A.; Eggins, B. R.; Brown, N. M. D.; McKinney, B.; Rouse, M. *J. Appl. Catal. B* **1998**, *17*, 25. (b) Mills, A.; Wang, J. *J. Photochem. Photobiol., A* **1998,** *118*, 53. (c) Mills, A.; Wang, J. *Int. J. Res. Phys. Chem. Chem. Phys.* **1999**, *213*, 49. (d) Kemp, T. J.; Unwin, P. R.; Vincze, L. *J. Chem. Soc., Faraday Trans.* **1995**, *91*, 3893. (e) Rideh, L.; Wehrer, A.; Ronze, D.; Zoulalian, A. *Catal. Today* **1999**, *48*, 357.

(3) (a) Mills, A.; Hunte, S. Le. *J. Photochem. Photobiol., A* **1997**, *108*, 1. (b) Mills, A.; Davies, R. H.; Worsley, D. *Chem. Soc. Rev.* **1993**, *22*, 417.

(4) (a) Ollis, D. F.; Pelizzetti, E.; Serpone, N. In *Photocatalysis*: *Fundamentals and Applications*; Serpone, N., Pelizzetti, E., Eds.; Wiley

Interscience: New York, 1989. (b) Ollis, D. F., Ekabi, H. A., Eds. *Photocatalytic Purification and Treatment of Water and Air*; Elsevier: New York, 1993.

(5) (a) Hoffmann, M. R.; Martin, S. T.; Choi, W.; Bahnemann, D. W. *Chem. Rev.* **1995**, *95*, 69. (b) Fox, M. A.; Dulay, M. T. *Chem. Rev.* **1993**, *93*, 34.

(6) (a) Upadhaya, S.; Ollis, D. F. *J. Phys. Chem. B* **1997**, *101*, 2625. (b) Sczechowski, J. G.; Koval, C. A.; Noble, R. D. *J. Photochem. Photobiol., A* **1993**, *74*, 273.

(7) Rideh, L.; Wehrer, A.; Ronze, D.; Zoulalian, A. *Catal. Today* **1999**, *48*, 357.

(8) Turchi, C. S.; Ollis, D. F. *J. Catal.* **1990** *122*, 178.

(9) Al-Ekabi, H.; Serpone, N. *J. Phys. Chem.* **1988**, *92*, 5726.

(10) Stafford, U.; Gray, K. A.; Kamat, P. V. *Res. Chem. Intermed.* **1997**, *23*, 355.

(11) (a) Gerischer, H.; Heller, A. *J. Phys. Chem.* **1991**, *95*, 5261. (b) Gerischer, H.; Heller, A. *J. Electrochem. Soc.* **1992**, *139*, 113. (c) Gerischer, H. *Electrochim. Acta* **1993**, *38*, 3. (d) Gerischer, H. *J. Phys. Chem.* **1991**, *95*, 1356.

(12) Wang, C.-M.; Heller, A.; Gerischer, H. *J. Am. Chem. Soc.* **1992**, *114*, 5230.

(13) Vinodgopal, K.; Stafford, U.; Gray, K. A.; Kamat, P. V. *J. Phys. Chem.* **1994**, *98*, 6797.

(14) Kormann, C.; Bahnemann, D. W.; Hoffmann, M. R. *Environ. Sci. Technol.* **1991**, *25*, 494.

(15) Bideau, M.; Claudel, B.; Faure, L.; Kazouan, H. *J. Photochem. Photobiol., A* **1991**, *61*, 269.

(16) Kesselman, J. M.; Shreve, G. A.; Hoffmann, M. R.; Lewis, N. S. *J. Phys. Chem.* **1994**, *98*, 13385.

(17) For example, see: (a) Unwin, P. R.; Barwise, A. J.; Compton, R. G. *J. Colloid Interface Sci.* **1989**, *128*, 208. (b) Compton, R. G.; Pritchard, K. L.; Unwin, P. R. *Chem. Commun.* **1989**, *249*. (c) Compton, R. G.; Unwin, P. R. *Philos. Trans. R. Soc., London, Ser. A* **1990**, *330*, 1. (d) Compton, R. G.; Pritchard, K. L. *Philos. Trans. R. Soc., London, Ser. A* **1990**, *330*, 47. (e) Brown, C. A.; Compton, R. G.; Narramore, C. A. *J. Colloid Interface Sci.* **1993**, *160*, 1517. (f) Compton, R. G.; Brown, C. A. *J. Colloid Interface Sci.* **1994**, *165*, 445.

(18) For reviews, see: (a) Unwin, P. R.; Macpherson, J. V. *Chem. Soc. Rev.* **1995**, *24*, 109. (b) Macpherson, J. V.; Unwin, P. R. *Prog. React. Kinet.* **1995**, *20*, 185. (c) Unwin, P. R. *J. Chem. Soc., Faraday Trans.* **1998**, *94*, 3183. (d) Unwin, P. R.; Compton, R. G. *Compr. Chem. Kinet.* **1989**, *29*, 173.

(19) For reviews, see: (a) Compton, R. G.; Dryfe, R. A. W. *Prog. React. Kinet.* **1995**, *20*, 245. (b) Cooper, J. A.; Compton, R. G. *Electroanalysis* **1998**, *10*, 141.

(20) (a) Cooper, J. A.; Wu, M.; Compton, R. G. *Anal. Chem.* **1998**, *70*, 2922. (b) Compton, R. G.; Barghout, R.; Eklund, J. C.; Fisher, A. C.; Davies, S. G.; Metzler, M. R.; Bond, A. M.; Colton, R.; Walter, J. N. *J. Chem. Soc., Dalton Trans.* **1993**, 3641. (c) Compton, R. G.; Barghout, R.; Eklund, J. C.; Fisher, A. C.; Davies, S. G.; Metzler, M. R. *J. Chem. Soc., Perkin Trans. 2* **1993**, 39.

(21) Ahmed, S.; Jones, C. E.; Kemp, T. J.; Unwin, P. R. *Phys. Chem. Chem. Phys.* **1999**, *1*, 5229.

(22) Buechter, K.; Nam, C. H.; Zawistowski, T. M.; Noble, R. D.; Koval, C. A. *Ind. Eng. Chem. Rev.* **1999**, *38*, 1258.

(23) Wu, T.; Liu, G.; Zhao, J.; Hidaka, H.; Serpone, N. *J. Phys. Chem. B* **1999**, *103*, 4862.

(24) Kormann, C.; Bahnemann D. W.; Hoffmann, M. R. *Environ. Sci. Technol.* **1988**, *22*, 798.

(25) Shibata, H.; Ogura, Y.; Sawa, Y.; Kono, Y. *Biosci. Biotechnol. Biochem.* **1998**, *62*, 2306.

(26) Matthews, R. W. In *Photochemical Conversion and Storage of Solar Energy*; Pelizzetti, E., Schiavello, M., Eds.; Kluwer: Netherlands, 1991; p 427.

(27) Sakai, H.; Baba, R.; Hashimoto, K.; Fujishima, A.; Heller, A. *J. Phys. Chem.* **1995**, *99*, 11896.

(28) Maeda, H.; Ikeda, K.; Hashimoto, K.; Ajito, K.; Morita, M.; Fujishima, A. *J. Phys. Chem. B* **1999**, *103*, 3213.

(29) Fonseca, S. M.; Barker, A. L.; Ahmed, S. A.; Kemp, T. J.; Unwin, P. R. *Chem. Commun.* Submitted for publication.

(30) Orton, R.; Unwin, P. R. *J. Chem. Soc., Faraday Trans.* **1993**, *89*, 347.

(31) Hatchard, C. G.; Parker, C. A. *Proc. R. Soc., London, Ser. A* **1956**, *235*, 518. (b) Vincze, L.; Kemp, T. J.; Unwin, P. R. *J. Photochem. Photobiol.* **1999**, *123*, 7.

(32) Pletcher, D.; Sotiopoulos, S. *J. Electroanal. Chem.* **1993**, *356*, 109.

(33) Rideh, L.; Wehrer, A.; Ronze, D.; Zoulalian, A. *Catal Today* **1999**, *48*, 357.

(34) Ahmed, S.; Kemp, T. J.; Unwin, P. R. *J. Photochem. Photobiol., A* **2001**, *141*, 69.

(35) Mills, A.; Wang, J. *J. Photochem. Photobiol., A* **1998**, *118*, 1.